Finanziato dall'Unione europea NextGenerationEU | Ministero dell'Università e della Ricerca | Italiadomani PIANO NAZIONALE DI RIPRESA E RESILIENZA

multi-Risk sciEnce for resilienT commUnities undeR a changiNg climate Codice progetto MUR: **PE00000005** – J33C22002840002

Deliverable title: Report with graphs and data tables on the impact and initial conditions of explosive eruptions from data of pyroclastic deposits

Deliverable ID: DV 3.3.2

Due date:31/03/2026

Submission date: 31/03/2026

AUTHORS

Federico Lucchi, Matteo Roverato, C.A.Tranne (UNIBO); Roberto Sulpizio (UNIBA); Raffaello Cioni (UNIFI); Paola Petrosino (UNINA)

1. Technical references

Project Acronym	RETURN
Project Title	multi-Risk sciEnce for resilienT commUnities undeR a changiNg climate
Project Coordinator	Domenico Calcaterra UNIVERSITA DEGLI STUDI DI NAPOLI FEDERICO II domcalca@unina.it
Project Duration	December 2022 – November 2025 (36 months)

Deliverable No.	DV3.3.2.
Dissemination level*	
Work Package	WP3.3 - Hazard and expected impact of explosive volcanoes
Task	T3.3.2.- Reverse engineering of pyroclastic deposits
Lead beneficiary	UNIBO
Contributing beneficiary/ies	UNIBA, UNIFI, UNINA.

* PU = Public

PP = Restricted to other programme participants (including the Ministry Services)

RE = Restricted to a group specified by the consortium (including the Ministry Services)

CO = Confidential, only for members of the consortium (including the Ministry Services)

Document history

Version	Date	Lead contributor	Description
0.1	20/02/2026	Federico Lucchi (UNIBO)	First draft
0.2			Critical review and proofreading
0.3			Edits for approval
1.0			Final version

2. ABSTRACT

This deliverable presents the results of Task 3.3.2 within WP3.3 of the RETURN project, focusing on the reverse engineering of pyroclastic deposits to reconstruct the initial conditions, dynamics, and impacts of explosive eruptions . Through an integrated multidisciplinary approach combining stratigraphic reconstruction, structural analysis, geochemical characterization, laboratory-based textural investigations, geochronology, and innovative three-dimensional imaging techniques, the study provides new constraints on both phreatic and vulcanian eruptive processes.

Case studies from Milos and Nisyros (Greece) improve the understanding of steam-driven explosions in low-enthalpy hydrothermal systems, highlighting the role of localized overpressure, structural control, and repeated shallow excavation processes, including rare large-magnitude phreatic events. Investigations at La Fossa cone (Vulcano Island, Italy) refine the eruptive model of vulcanian activity, emphasizing magma plug dynamics, volatile exsolution, and the predominance of dense ballistic ejecta as indicators of conduit evolution. The three-dimensional characterization of volcanic ash aggregates provides new quantitative parameters essential for improving atmospheric ash transport and dispersal models.

Finally, high-resolution tephrostratigraphic analyses in the Neapolitan volcanic district refine eruption chronologies, identify previously unrecognized eruptive events, and clarify both direct and indirect environmental and societal impacts of explosive volcanism.

Overall, the results contribute to strengthening conceptual models of eruption triggering, constraining eruptive parameters and recurrence patterns, and improving the scientific basis for volcanic hazard assessment and risk mitigation strategies.

3. Table of contents

1. Technical references 3
1.1. Document history 4
2. Abstract 6
3. Table of contents 5
3.1. List of Tables 6
3.2. List of Figures 7
4. First Section - UNIBO, UNIBA 8
4.1. Historical small-scale phreatic eruptions at Milos Island (Greece) as seen from geological and archaeological investigations 8
4.2. Phreatic Explosion Dynamics and Hydrothermal System Evolution at Nisyros Caldera 10
4.3. Giant phreatic eruptions at Milos Island (Greece) 13
4.4. Analytical study of pyroclasts documenting 800 years of eruptive activity at La Fossa cone, Vulcano Island 14
5. Second Section - UNIFI 16
5.1. 3D structure and characteristics of volcanic ash aggregates 16
5.2. Eruptive conditions and dynamics of activity of La Fossa volcano (Vulcano Island, Italy) during the 1888-1890 eruption from the study of the ballistic bomb field 17
5.3. Non-explosive vs. explosive magma fragmentation during the 1888-90 eruption of La Fossa (Vulcano, Eolian Islands): insights from breccia-bearing blocks 20
5.4. A revised model for the dynamics of vulcanian activity through a comparative analysis of vulcanian ballistic bomb fields from three different volcanoes 21
6. Second Section - UNINA 23
6.1. Refining the Late Quaternary tephrostratigraphic framework of the Neapolitan volcanic district from a marine core in the Gulf of Salerno (Tyrrhenian Sea) 23
6.2. Unravelling 6000 years of interplay among environmental changes, anthropogenic activities, and Vesuvius eruptions in the upper Sarno Plain (Campania, Italy) 27
7. Conclusions 30
6. References 32

List of Tables

Table 1 - Summary of modelled ages attributed to each cryptotephra using the refined age model, along with their inferred volcanic sources and associated eruptive events. SV= Somma-Vesuvius; CF= Campi Flegrei; IS= Ischia; Pr= Procida; Et= Etna.

Table 2: Summary of the attribution of the primary and reworked tephra embedded in the San Vito sequence, with the age constraints derived from tephrostratigraphic analysis. Abbreviations: Tr=trachyte; Tr-ph=

trachy-phonolite; Ph=phonolite; Tph=tephriphonolite; Ph-teph=phonotephrite; Foi=foidite. [(1)]Santacroce et al. (2008); [(2)]Giaccio et al. (2017); [(3)]Passariello et al. (2009); [(4)]Smith et al. (2011); [(5)]Totaro et al. (2022) and references therein.

List of Figures

Figure 1: *Polarized light microscope fabric observations of volcanic material from the samples of phreatic deposits on Milos, and XRD spectra of one sample MIL21-20 showing the presence of the bright and dark opaline bands*

Figure 2: *Sketch of the different stages of the geothermal system and phreatic activity at Milos Island.*

Figure 3: *Schematic geological map of the summit phreatic crater field of Nisyros (Greece)*

Figure 4: *Correlation of stratigraphic sections showing the main relationships between distinct phreatic units and volcaniclastic infilling deposits in the Kaminakia-Stefanos and Polyvotis-Lofos crater fields in the summit caldera of Nisyros Island.*

Figure 5: *Example of the Green Lahar deposit at an outcrop where two distinct units overlie an altered rhyolitic dome. On the right, a close-up shows the material composing the two units*

Figure 6: *Examples of juvenile fragments of the PIetre Cotte succession displaying angular, fractured glassy shapes, typical of phreatomagmatic fragmentation, and/or elongated vesicular morphologies related to magmatic degassing. Surface alteration due to acidic fluids interaction (chemical pitting) is also observed in several samples.*

Figure 7: *Internal structure, componentry and porosity spatial distribution of the different types of ash aggregates studied.*

Figure 8: *Vesicle features, internal density gradient and vesicle size distribution of the different types of blocks and bombs recognized in this study*

Figure 9: *Examples of breccia-bearing blocks (top); SEM backscattered image of the brecciated portion of the block (middle); results of the analysis of orientation of the maximum Feret of the different clasts (bottom).*

Figure 10: *The proposed, alternative models of vulcanian activity*

Figure 11: ***a)** Isotopic record of the Greenland NGRIP ice core (Rassmussen et al., 2014) and **b)** Sea Surface Temperatures (SSTs) recorded by alkenones at ODP Site 976 in the Alboran Sea (Martrat et al., 2014), in relation to **c)** the percentage abundance of warm water species Globigerinoide ruber (Jamka, 2019) and **d)** SSTs recorded by planktonic foraminiferal assemblages of the C106 core (Di Donato et al., 2019); **e)** Magnification of the 300–400 cm interval of the core, in which the identified cryptotephra (orange lines and sample codes) and the levels where the glass fraction is absent or very low in relation to the non-volcanic component (purple lines) are evident. The beige shading defines Heinrich Stadial HS1 and gray shading layer H1.1 (from Hodell et al., 2017). The yellow shading highlights the deposition of the "precursors of the Neapolitan Yellow Tuff" and of the NYT itself.*

Figure 12: *Left: type section of the pyroclastic fall deposits cropping out in upper Sarno Plain. The thickness of the single layers is the maximum recorded in the area. Right: plot of the eruptions found in the San Vito succession; red flag=primary tephra (mono-component); yellow flag= reworked tephra (poly-component).*

4.First Section – UNIBO, UNIBA

4.1 Historical small-scale phreatic eruptions at Milos Island (Greece) as seen from geological and archaeological investigations

4.1.1 Aims

Phreatic and hydrothermal eruptions are among the most hazardous volcanic phenomena due to their limited predictability. Milos Island, with its low-enthalpy hydrothermal system that produced hundreds of small phreatic cones in its southeastern sector, offers an ideal natural laboratory to investigate these processes. The aims of the study are to:

- Characterize the morphology, spatial distribution, and products of the phreatic craters on Milos.
- Identify the geological and hydrothermal conditions that controlled their formation.
- Develop a conceptual model for the triggering of phreatic eruptions in low-enthalpy hydrothermal systems.
- Provide insights that can be applied to similar active hydrothermal settings worldwide.

4.1.2 Research outcomes

Our investigation of the phreatic field on Milos Island identified more than 250 small craters, most of which are less than 100 m in diameter and commonly occur as nested structures rather than isolated features. Their distribution and morphology, together with stratigraphic evidence, reveal that they were produced by repeated shallow phreatic explosions. Geochemical analyses of both the fragmented ejecta and the underlying substrate indicate that these events were associated with a low-enthalpy hydrothermal system, with temperatures generally between 100 and 300 °C and local peaks up to 370 °C. The estimated explosion energies (10^{10}–10^{12} J) and excavation depths (2–10 m) are consistent with rapid steam-driven fragmentation occurring at very shallow levels.

By integrating morphometric, spatial, stratigraphic, and geochemical data, we developed a conceptual model that explains the triggering mechanisms of phreatic eruptions on Milos. This model highlights the role of localized pressurization within the hydrothermal system and the importance of structural pathways in focusing eruptive activity. When combined with archaeological and historical evidence, these findings provide a coherent framework for interpreting past phreatic activity on the island. Overall, the outcomes of this study contribute to a broader understanding of how low-enthalpy hydrothermal systems can generate repeated small-scale phreatic eruptions. The insights gained from Milos offer valuable guidance for evaluating hazards in analogous active hydrothermal settings worldwide.

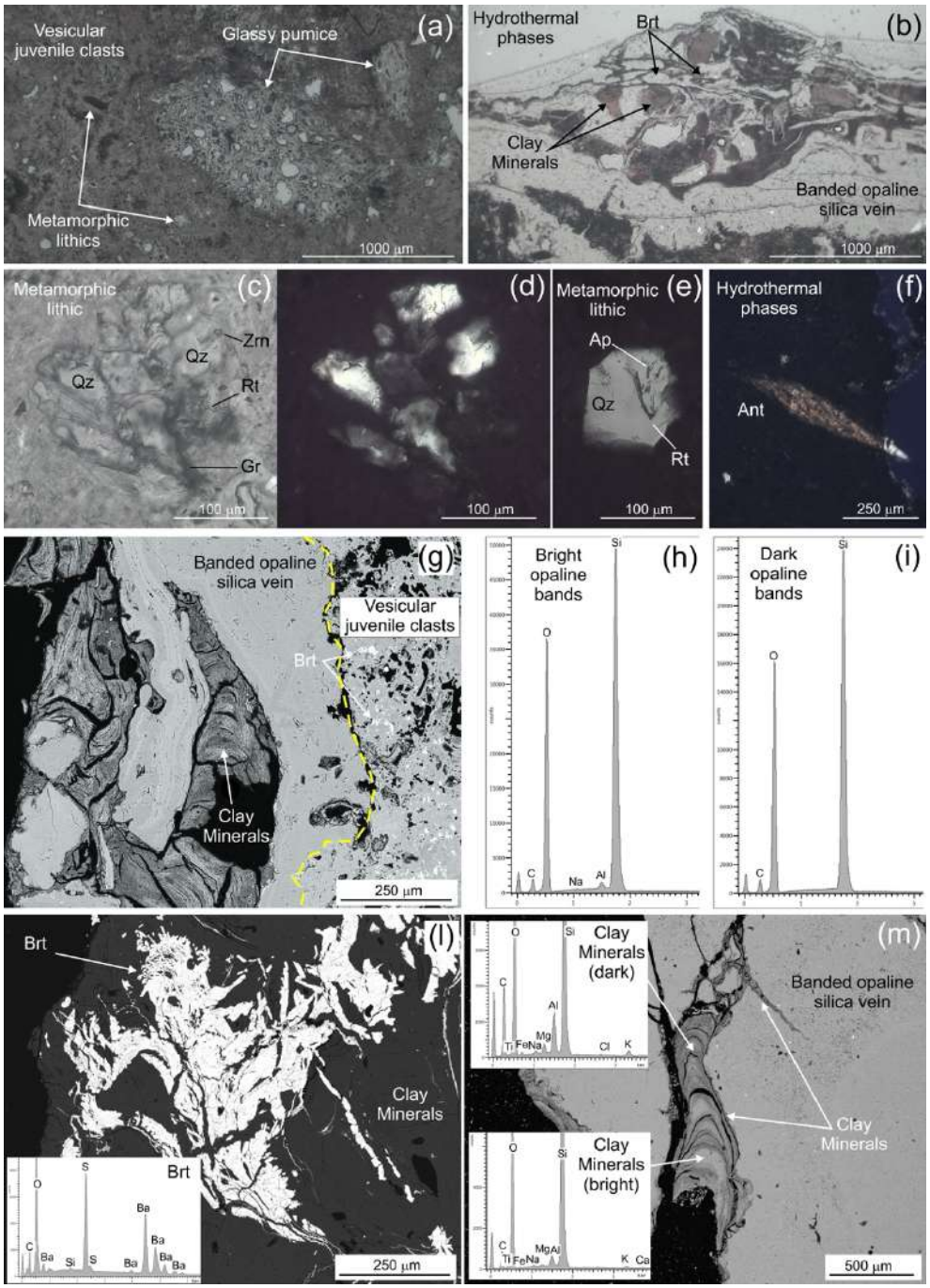

Figure 1: *Polarized light microscope fabric observations of volcanic material from the samples of phreatic deposits on Milos, and XRD spectra of one sample MIL21-20 showing the presence of the bright and dark opaline bands*

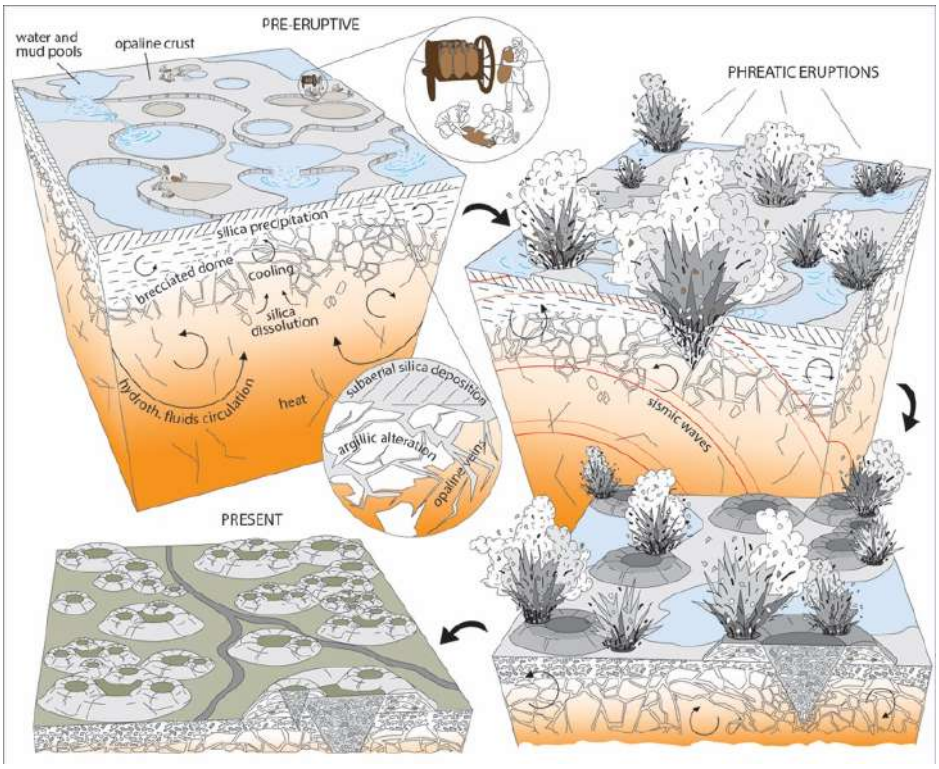

Figure 2: *Sketch of the different stages of the geothermal system and phreatic activity at Milos Island.*

4.2 Phreatic Explosion Dynamics and Hydrothermal System Evolution at Nisyros Caldera

4.2.1 Aims

To improve the understanding of shallow hydrothermal systems and the processes leading to phreatic explosions in active volcanic settings. Within this framework, the activity conducted at Nisyros Island (Greece) focuses on reconstructing the stratigraphic, structural and historical evolution of steam-driven explosive events in order to constrain their recurrence, magnitude and triggering mechanisms.

The main objectives of the Nisyros study are:

(i) to develop a detailed stratigraphic reconstruction of historical phreatic deposits within the Lakki caldera;

(ii) to identify and characterize individual explosion units and associated craters through integrated field mapping and UAV-based photogrammetry;

(iii) to investigate the structural control on vent localization and hydrothermal circulation;

(iv) to estimate key eruptive parameters (e.g., excavation depth, ballistic dispersal, deposit distribution) relevant for hazard assessment;

(v) to integrate geological evidence with a critical revision of historical sources in order to refine the chronology of phreatic activity.

This multidisciplinary approach contributes to the broader goals of strengthening conceptual models of hydrothermal sealing, overpressure development and explosive failure in steam-driven systems.

4.2.2 Research outcomes

The research carried out at Nisyros led to the identification and mapping of twelve lithostratigraphic units related to phreatic activity, grouped into two main crater fields: Kaminakia–Stefanos and Polyvotis–Lofos. The integration of detailed fieldwork with UAV-derived orthophotos and DEMs allowed reconstruction of crater morphology, cross-cutting relationships and deposit distribution, significantly refining previous models. Stratigraphic evidence indicates that major craters such as Stefanos and Megalos Polyvotis are composite structures formed by multiple closely spaced explosions. Ballistic dispersal patterns and impact structures provided constraints on explosion energy and vent geometry, revealing variability in eruptive magnitude across different events. Structural analysis highlighted a strong tectonic control on vent distribution, with explosions preferentially localized along NE–SW fault systems or along the margins of pre-existing craters. The re-evaluation of historical accounts enabled correlation between mapped deposits and documented 19th-century explosions, improving the recent eruptive chronology of the island. Overall, the Nisyros case study provides an integrated volcanological and structural framework for understanding phreatic activity in caldera-hosted hydrothermal systems and supports improved assessment of related volcanic hazards.

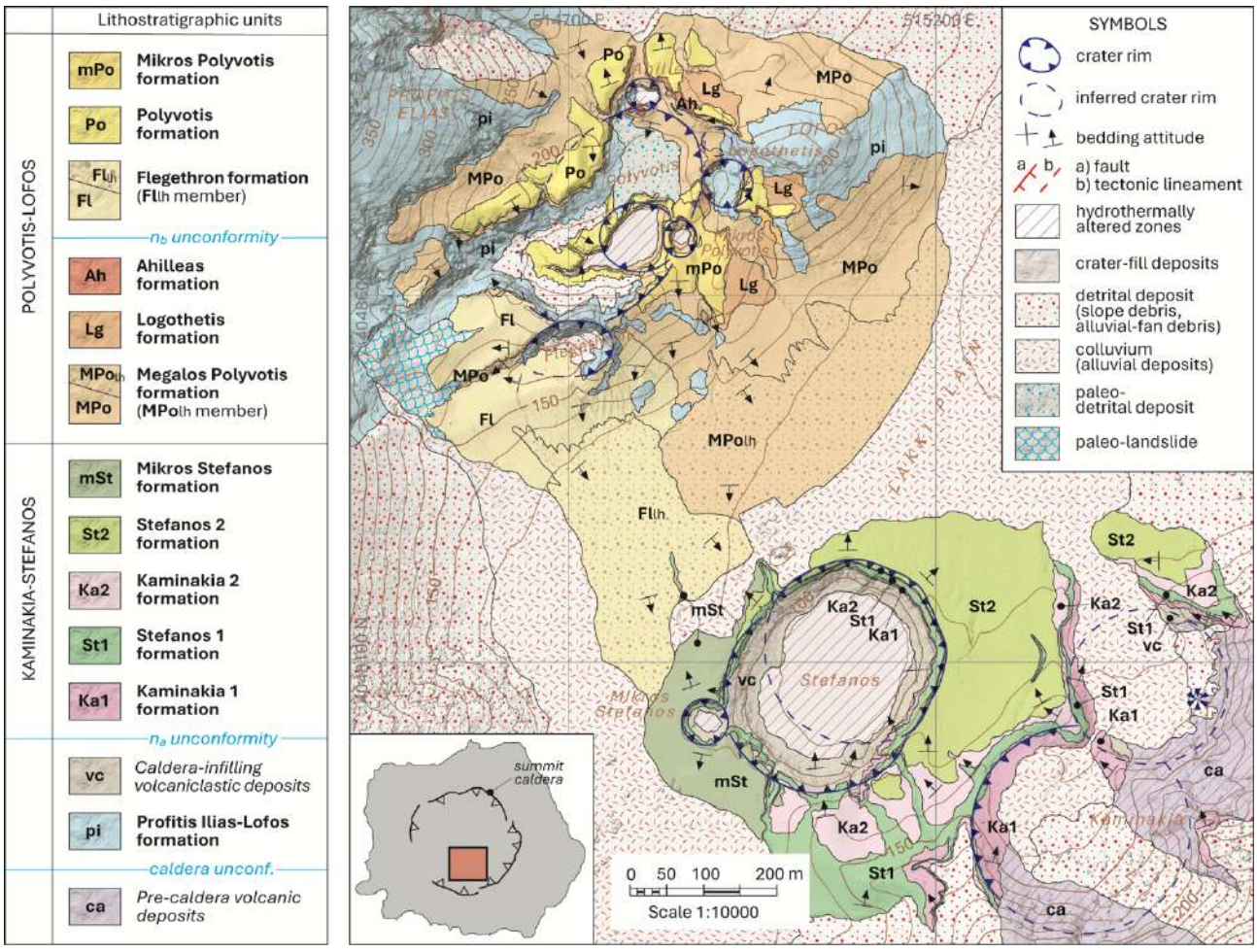

Figure 3: Schematic geological map of the summit phreatic crater field of Nisyros (Greece)

Finanziato dall'Unione europea NextGenerationEU
Ministero dell'Università e della Ricerca
Italiadomani PIANO NAZIONALE DI RIPRESA E RESILIENZA

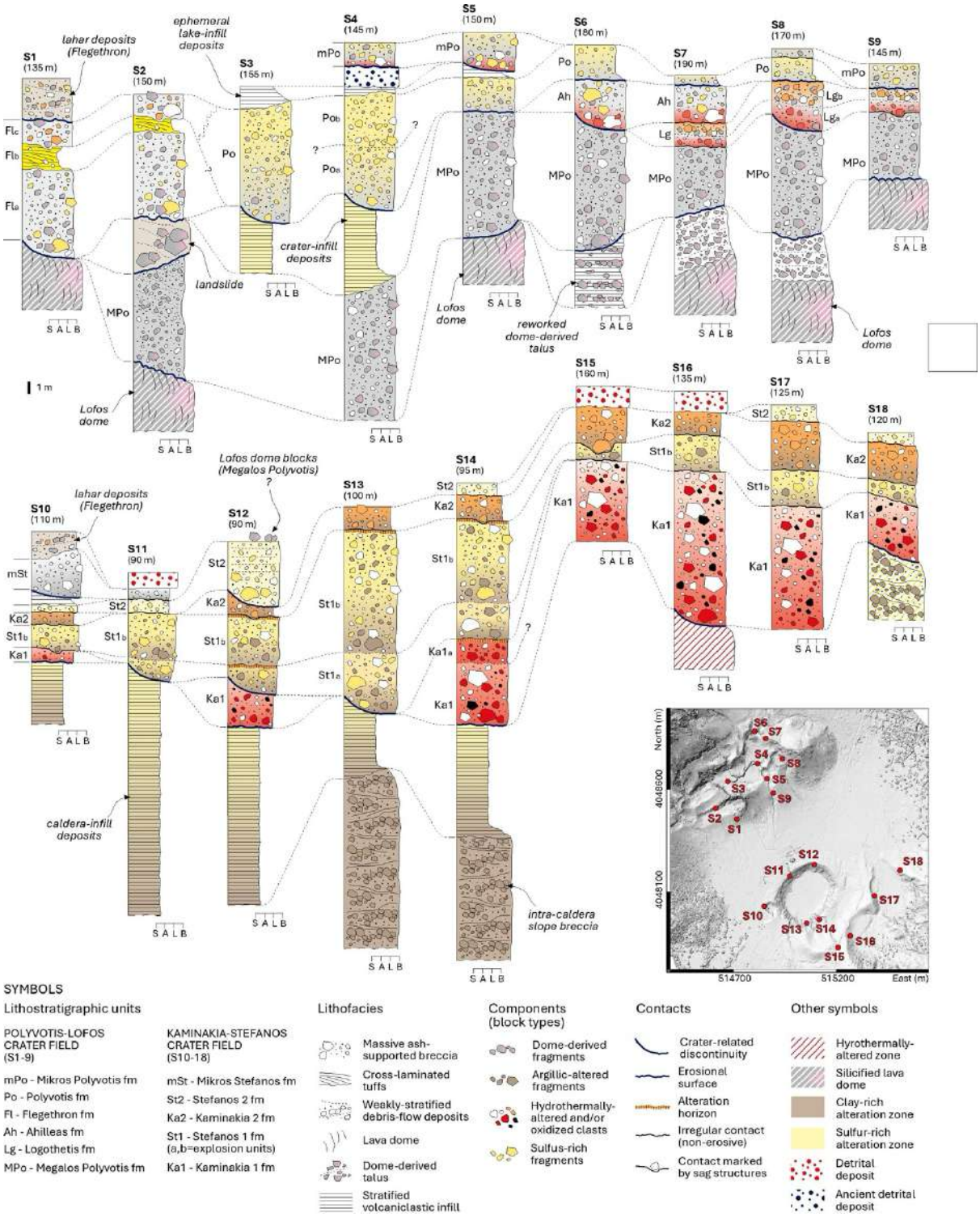

Figure 4: *Correlation of stratigraphic sections showing the main relationships between distinct phreatic units and volcaniclastic infilling deposits in the Kaminakia-Stefanos and Polyvotis-Lofos crater fields in the summit caldera of Nisyros Island.*

4.3 Giant phreatic eruptions at Milos Island (Greece)

4.3.1 Aims

In another sector of Milos Island, a second hydrothermal system—distinct in many aspects from the one previously described—provides yet another ideal natural laboratory for investigating phreatic explosions. We focused our work on a phreatic eruption that produced the so-called *Green Lahar* deposit (a misleading name because the deposit was not formed by a lahar process), representing one of the largest phreatic events worldwide known to date.

The objectives of the study are to:

- Determine the geological framework and hydrothermal conditions that controlled the formation of the Green Lahar deposit.
- Describe and analyze the morphology, spatial distribution, and eruptive products associated with the phreatic event.
- Develop a conceptual model for the initiation of phreatic eruptions in low-enthalpy hydrothermal systems.
- Provide insights that can be applied to other similar active hydrothermal environments worldwide.

4.3.2 Research outcomes

Our investigation highlights that phreatic eruptions represent some of the most dangerous and least understood volcanic phenomena, driven by the rapid vaporization of subsurface water and the abrupt conversion of thermal energy into mechanical work. We documented extensive hydrothermal activity in the eastern sector of the island, where geological conditions strongly favor phreatic explosions. Building on previous knowledge of Pleistocene phreatic phases, our work has identified at least two exceptionally large phreatic eruptions of uncertain age (between ~100 ka and 1 Ma), originating within the Mesozoic–Palaeogene metamorphic basement. These eruptions produced thick eruptive units—up to 50 m—composed of extremely poorly sorted, clast-supported angular lapilli and blocks (up to 1 m), predominantly derived from schistose country rock. We interpret these deposits as very proximal fallout and widespread pyroclastic density currents covering at least 15 km² on land, with maximum runout distances of 7 km from their inferred sources. The scale and distribution of these deposits suggest that these events rank among the largest phreatic eruptions currently known.

Collectively, these findings expand the recognized spectrum of phreatic eruption magnitudes and emphasize the potential for giant steam-driven events in low-enthalpy hydrothermal settings. Ongoing and future analyses aim to refine our understanding of the subsurface conditions controlling fluid pressurization, host-rock behavior, and the ultimate triggering mechanisms responsible for these exceptional eruptions.

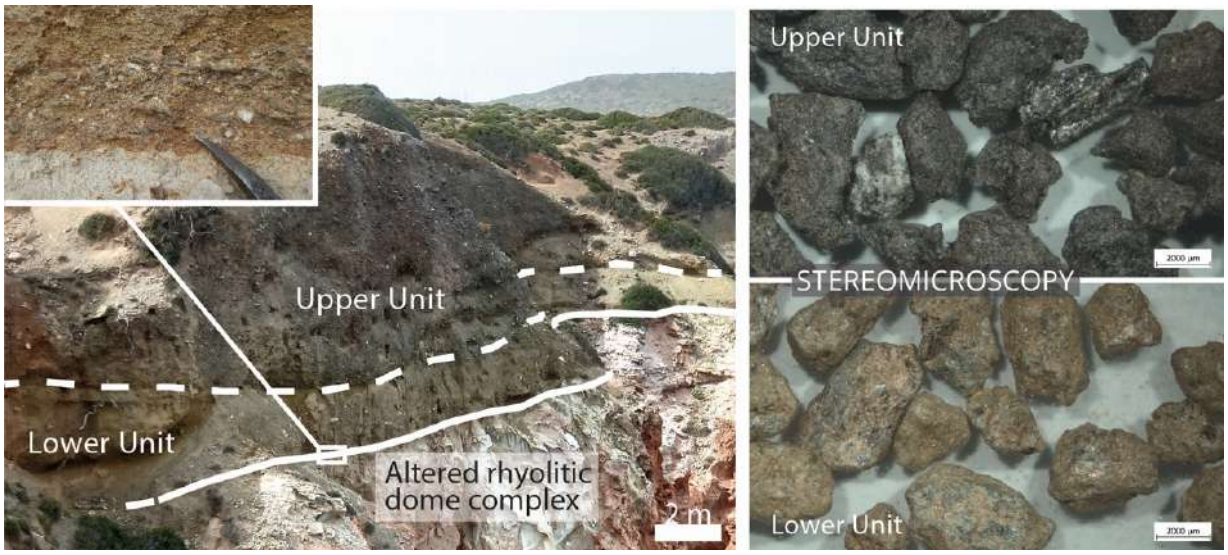

Figure 5: *Example of the Green Lahar deposit at an outcrop where two distinct units overlie an altered rhyolitic dome. On the right, a close-up shows the material composing the two units*

4.4 Analytical study of pyroclasts documenting 800 years of eruptive activity at La Fossa cone, Vulcano Island

4.4.1 Aims

The main goal of the present project is to define the mechanisms that govern the initial stages of explosive eruptions, with particular attention to the processes driving vent opening and early eruptive transitions. By integrating field observations, laboratory analyses, and numerical or conceptual modeling, the project seeks to better constrain the dynamics of the shallow magmatic–hydrothermal system over the last <1000 years of activity. These insights will ultimately support a more robust assessment of volcanic hazards at Vulcano Island and improve our ability to anticipate future eruptive scenarios.

4.4.2 Research outcomes

This work provides a refined reconstruction of the late Holocene (<1000 years) stratigraphy of the La Fossa cone (Vulcano), with an emphasis on the Pietre Cotte pyroclastic succession and the overlying AD 1888–90 eruptive products, themselves superposed on the Commenda Formation (AD 1240–1300). Integrated field-based stratigraphic mapping, detailed volcanological facies analysis, and comprehensive laboratory investigations—including characterization of juvenile components, EMPA glass geochemistry, and SEM-based morphoscopic assessment—allow us to establish an updated eruptive succession produced by recurrent hydromagmatic-to-magmatic activity initiated by vent-opening phreatic phases. These eruptive dynamics generated multiple fallout and pyroclastic-density-current units, including at least two compositionally and texturally distinctive pumice-fall deposits, as well as the emplacement of the Pietre Cotte rhyolitic lava flow. Geochemical data demonstrate—and in part corroborate earlier findings—that the Pietre Cotte succession comprises two compositionally discrete magma batches, separated by a compositional gap that is bridged by the products of the AD 1988–90 activity.

This configuration strongly suggests late-stage magma mixing or mingling processes, further evidenced by banded juvenile clasts exhibiting sharply contrasting glass chemistries. Additionally, critical re-evaluation of historical documentation enables the proposal of a revised eruptive chronology that better constrains the temporal and genetic relationships among the principal explosive and effusive events of the Pietre Cotte cycle. This refined timeline provides an improved framework for assessing future eruptive scenarios and associated hazards at the La Fossa cone.

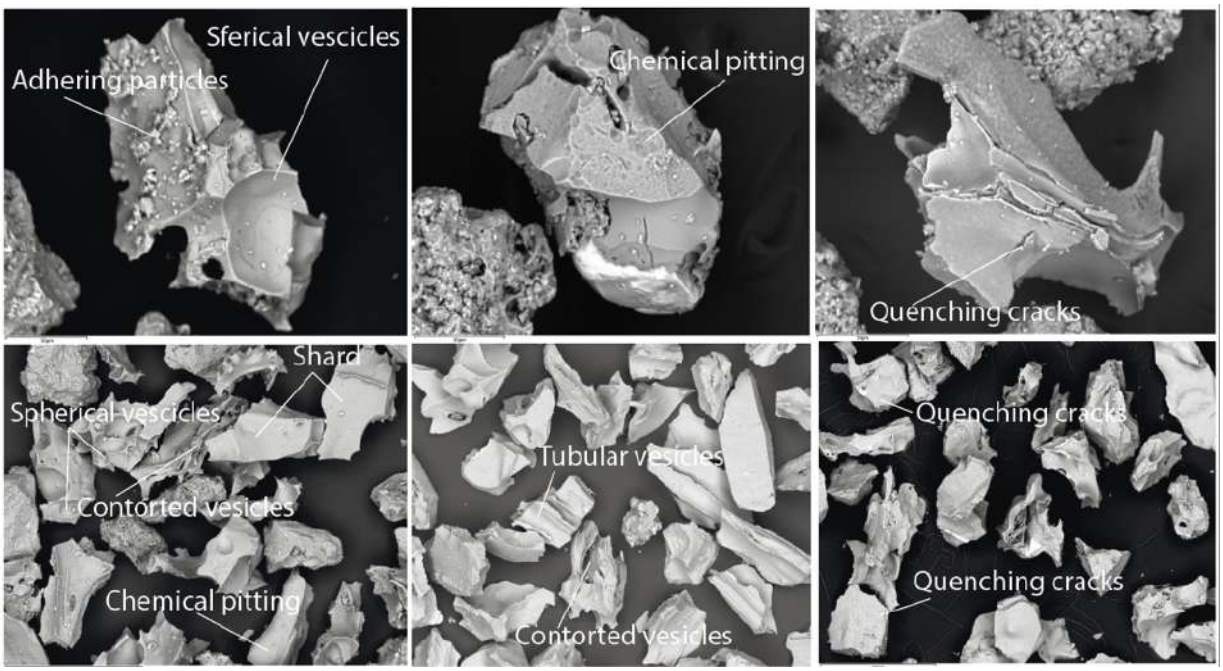

Figure 6: *Examples of juvenile fragments of the Pietre Cotte succession displaying angular, fractured glassy shapes, typical of phreatomagmatic fragmentation, and/or elongated vesicular morphologies related to magmatic degassing. Surface alteration due to acidic fluids interaction (chemical pitting) is also observed in several samples.*

5.Second Section - UNIFI

5.1 3D structure and characteristics of volcanic ash aggregates

5.1.1 Activity goals

Ash aggregation is a common process which characterize ash transport and dispersal in atmospheric volcanic plumes related to eruptions of variable intensity. Times of ash permanence in the atmosphere, and hence distances of ash dispersal, are strongly conditioned by mechanisms of ash aggregation, and present numerical models can only partially account for this process. This research gives for the first time first-hand data on physical and textural features of ash aggregates which can be used to constrain transport and dispersal models.

5.1.2 Main results

The primary objective of the study was to characterize in detail the internal structure and morphology of the different types of volcanic ash aggregates formed in a volcanic plume and/or in the volcanic cloud as a consequence of atmospheric tephra transport. These aggregates significantly influence sedimentation dynamics, the residence time of ash in the atmosphere, and, consequently, the forecasting of atmospheric fine tephra dispersal, with major implications on human health, civil activities and environmental impact. As volcanic aggregates are known to be extremely fragile and rarely preserved in deposits with intact airborne structures, studying their original three-dimensional external morphology and internal structure was up to now challenging for researchers, and accurate data were up to now not available especially for the most fragile and delicate aggregates categories (eg. Particle Clusters). We developed an innovative methodology us to fully preserve the airborne structures of the aggregates, capturing falling aggregates in UV-sensitive resins and filming them with high-speed cameras. The different aggregates were then observed using high-resolution X-ray tomography and reconstructed through an appositely written MatLab script, so defining their internal strcture, external shape, porosity and density. This disclosed the possibility to directly investigate and measure the physical and structural characteristics of natural aggregates, allowing for the first time the observation of the natural internal structure of the aggregates. Using this method, we were able to identify and characterize between the others also cored Ash Pellets (cAP1), a new type of aggregate never observed before, a significant advancement in the classification of volcanic aggregates and in the understanding of aggregation processes under natural conditions. The obtained results can be used to better understand the mechanisms of aggregates formation (electrostatic, collisional, or water-mediated), to implement numerical models with accurate parametric data collected on real ash aggregates, to refine atmospheric dispersion forecasts during volcanic eruptions aimed at preventing from hazards to distal areas or to aviation.

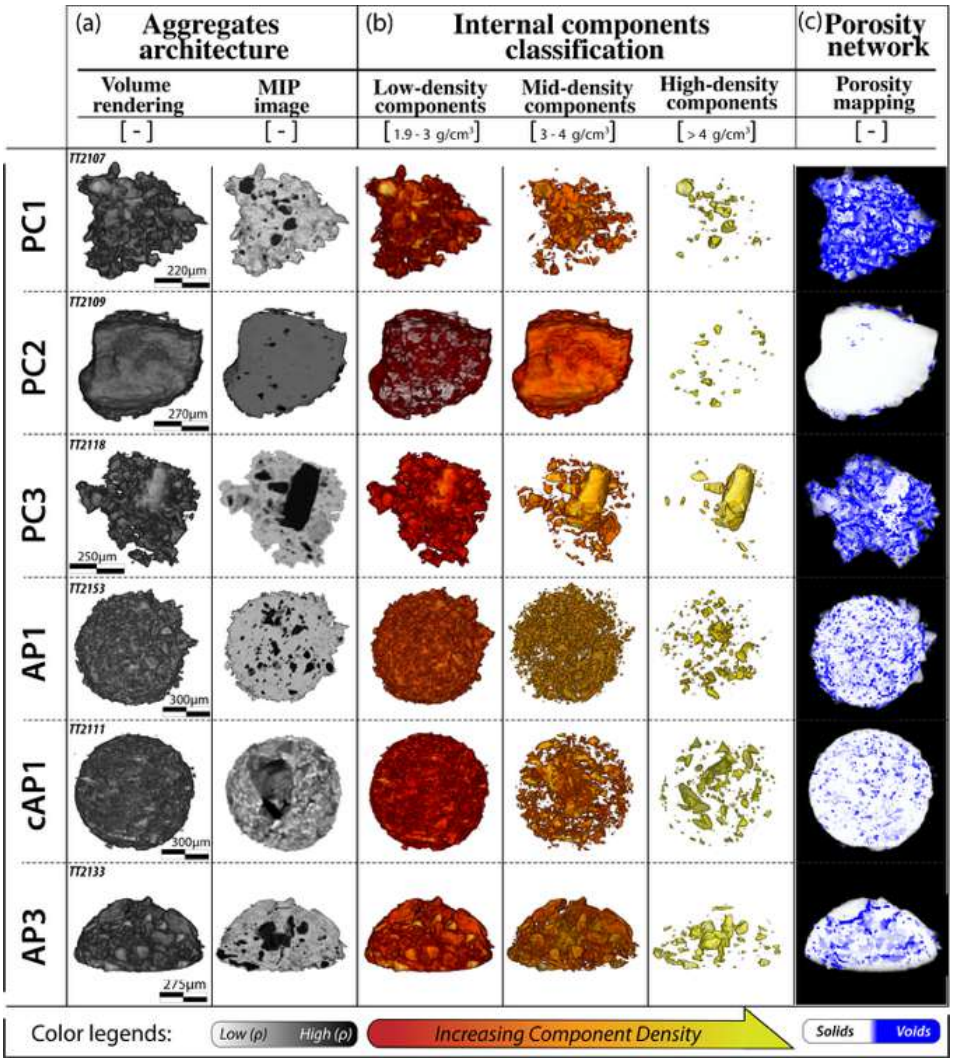

Figure 7: *Internal structure, componentry and porosity spatial distribution of the different types of ash aggregates studied.*

5.2 Eruptive conditions and dynamics of activity of La Fossa volcano (Vulcano Island, Italy) during the 1888-1890 eruption from the study of the ballistic bomb field

5.2.1 Activity goals

The physical, textural and petrological characteristics of the coarse ballistic fragments ejected during the 1888-90 vulcanian eruption of La Fossa volcano record the internal structure of the magma conduit plug which characterized the activity. The dispersal of ejecta and mass relations between the different types reflect the dynamics of the largest events which punctuated the eruption and can be used to better define hazards and impact parameters related to this type of eruptions.

5.2.2 Main results

The primary focus of this work was to provide a detailed physical description of the ballistic field resulting from the 1888-1890 eruption at La Fossa di Vulcano (Aeolian Islands) and still present in the crater area,

and to retrieve textural data on the different types of produced ballistics. After fieldwork activity aimed at mapping and quantifying the different ejecta occurring on the entire crater terrace, the study was focused on the nature, grain size, internal structure, and spatial dispersion of the ballistic products.

Six main types of bombs were distinguished, based on their internal and external morphological-textural characteristics, including:

- Dense blocks [D] and Dense blocks containing breccias [D-Br].

- Breadcrust bombs [BcB] (with three subcategories).

- Black Scoria bombs [S].

As also confirmed by the number of identified lithotypes, a wide variability was found in the morphological and textural characteristics of the bombs. Contrary to what is classically reported in the literature for this type of activity, dense blocks (D and Dbr) represent a dominant fraction of the deposit (up to 85 Wt% of the total). All these types of ejecta can be interpreted in terms of vertical and lateral gradients of vesicularity, crystallinity and hence rheology of a magma plug continuously occupying the upper conduit during the eruption, The classic Breadcrust Bombs (BcB) constitute only 20-25 Wt% of the total deposit. The spatial distribution of the various identified lithotypes proved to be markedly non-homogeneous and variable at the scale of the crater terrace.

These data allowed us to interpret the eruptive dynamics of the event. The variability in grain size and dispersion suggests the presence of repeated eruptive pulses distributed in preferential directions, indicating strongly non-stationary dynamics of the eruption. The relative abundance of the different products, combined with the long duration of the ballistic launch phase, indicate that the primary process driving this phase is likely the local pressurization and only partial fragmentation of the magma plug, due to the gradual and continuous loss of volatiles from the underlying magmatic conduit. These would also indicate slow ascent dynamics of a high-viscosity, pressurized, and partially degassed magma lying within the active syn-eruptive conduit of Vulcano.

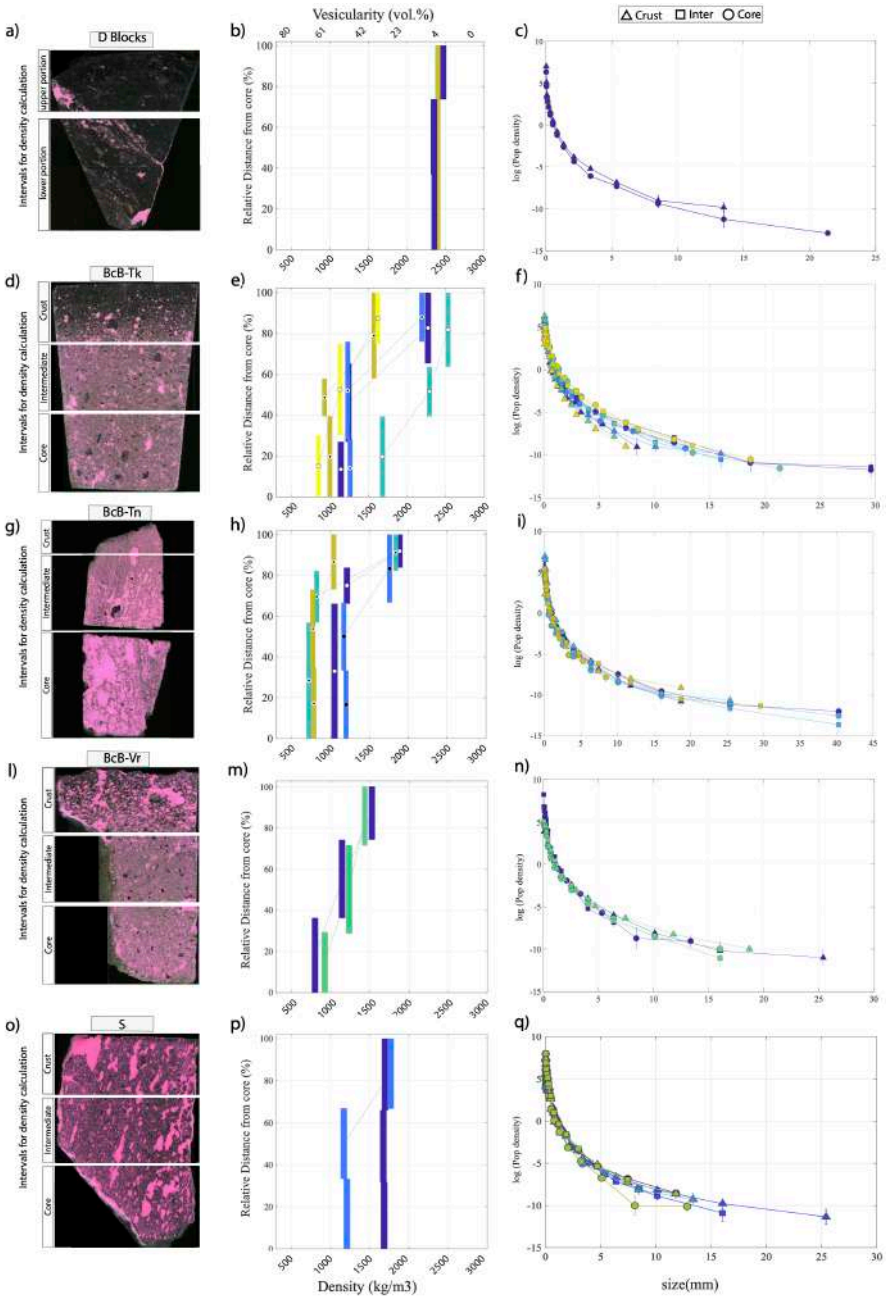

Figure 8: *Vesicle features, internal density gradient and vesicle size distribution of the different types of blocks and bombs recognized in this study*

5.3 Non-explosive vs. explosive magma fragmentation during the 1888-90 eruption of La Fossa (Vulcano, Eolian Islands): insights from breccia-bearing blocks

5.3.1 Activity goals

Peculiar breccia-bearing blocks found among the ballistic coarse ejecta of the 1888-90 vulcanian eruption of La Fossa volcano suggest the existence of a permeable network of fracture filled by mechanically abraded ash fragments in the magma plug, responsible of syn-eruptive degassing and emission of fine-grained material during low intensity explosions. Textural, morphological and compositional data of the fracture-filling ash support this interpretation, possibly a common process in plug-related, low-intensity, high-frequency vulcanian activity.

5.3.2 Main results

Vulcanian activity is characterized by the repeated occurrence, over a large range of timescales, from minutes to weeks, of explosions which release large amounts of gas and ash and ballistically eject coarse fragments. Resulting fragments are generally associated to the explosive partial disruption of domes or plug structures. The 1888-90 eruption of La Fossa volcano (Vulcano, Eolian Islands), the prototype of Vulcanian eruptions, was masterfully described Mercalli and De Fiore (1890) as a sequence of large explosions scattered during prolonged phases of lower intensity activity, characterized by high frequency small outbursts (up to hundreds events/day). This poses important questions about the dominant mechanism of magma fragmentation. In the present crater area, still covered by the bomb field of the 1888-90 eruption, dense blocks presenting a network of fractures filled with brecciated material are quite frequently recognized. Fracture-infilling fragments have been studied in detail through the characterization of their textural, compositional and morphological features. These are interpreted as the product of mechanical, shear-related fracturing of the rigid, hot upper portion of the plug, during the repeated events of plug pressurization. This type of fragmentation strongly contrasts with the explosive fragmentation mechanisms typical of the ash produced during the most intense activity. Active transport through the fracture network is suggested by the presence of clasts derived from the shattering of different portions of the plug. We suggest that gas-driven elutriation of ash present in the fracture network could have been responsible of most of ash emission during the low intensity phases, during which an extended primary fragmentation of the magma was inhibited.

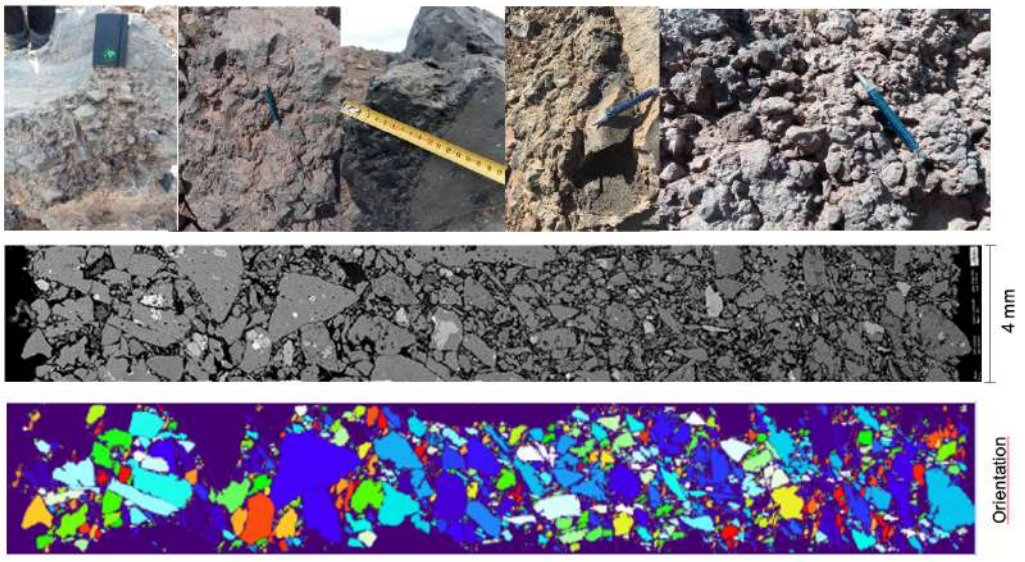

Figure 9: *Examples of breccia-bearing blocks (top); SEM backscattered image of the brecciated portion of the block (middle); results of the analysis of orientation of the maximum Feret of the different clasts (bottom).*

5.4 A revised model for the dynamics of vulcanian activity through a comparative analysis of vulcanian ballistic bomb fields from three different volcanoes

5.4.1 Activity goals

A model for the dynamics and pre- and syn-eruptive conditions typical of small-size vulcanian activity has been elaborated basing on the comparison of the analysis of coarse ballistic ejecta related to the 1888-90 eruption of La Fossa volcano (Eolian Islands, Italy), the 2014 eruption of Tungurahua volcano (Ecuador) and the 1999 eruption of Guagua Pichincha (Ecuador) already studied by our group. The results can represent a reference model for a future reactivation of La Fossa volcano.

5.4.2 Main results

Vulcanian eruptions are typically associated with the launch of different types of cm-to-m sized ballistic ejecta and with the production of large amount of ash typically transported by transient atmospheric plumes. Vulcanian explosions typically involve the expulsion of various types of coarse ballistic ejecta, characterized by variable shapes, internal and external textures, and vesicularity. The textural features of these ejecta can provide clues to understanding the temporal and spatial changes in conduit structure and illuminate the complex interactions among conduit processes, such as magma vesiculation, crystallization, and fragmentation, which play a crucial role in the erratic behaviour of these eruptions. The comparison of the morpho-textural and dispersal features of the products associated to three significant eruptions controlled by a clear vulcanian-like dynamics of the activity (the 1888-90 eruption at La Fossa Cone of Vulcano, the 1th February 2014 eruptive event at Tungurahua volcano, and the September-December 1999 activity of Guagua Pichincha volcano) aims to underscore the typical features commonly linked to Vulcanian activity and to demonstrate the key insights that can emerge from the analysis of these products. Strong similarities are evidenced among all the considered case-studies. Despite the presence of bread-crust bombs has been considered as peculiar of this activity, in all these cases dense, microlite-rich blocks are dominant between all the products, This clearly indicates that the formation of a dense, nearly totally degassed upper portion of a magma plug is the dominant process driving the eruption. The rapid formation of such magma portion represents a “sine qua non” condition for progressive gas accumulation and the occurrence of repeated explosions, so clearly indicating a bottom-up onset of fragmentation that can then extend below the initial fragmentation depth through a downward propagating decompression wave. The textural features of vulcanian bombs well describe the time-space evolution of conduit stratigraphy and shed light on the complex interplay between the different conduit processes that actively control the unsteady dynamics of vulcanian eruptions. The comparison between different types of vulcanian activity clearly demonstrates the existence of a spectrum of activity characterized by different intensity and frequency of explosions, that should be considered while establishing expected eruption scenarios in case of reactivation at Vulcano Island or elsewhere.

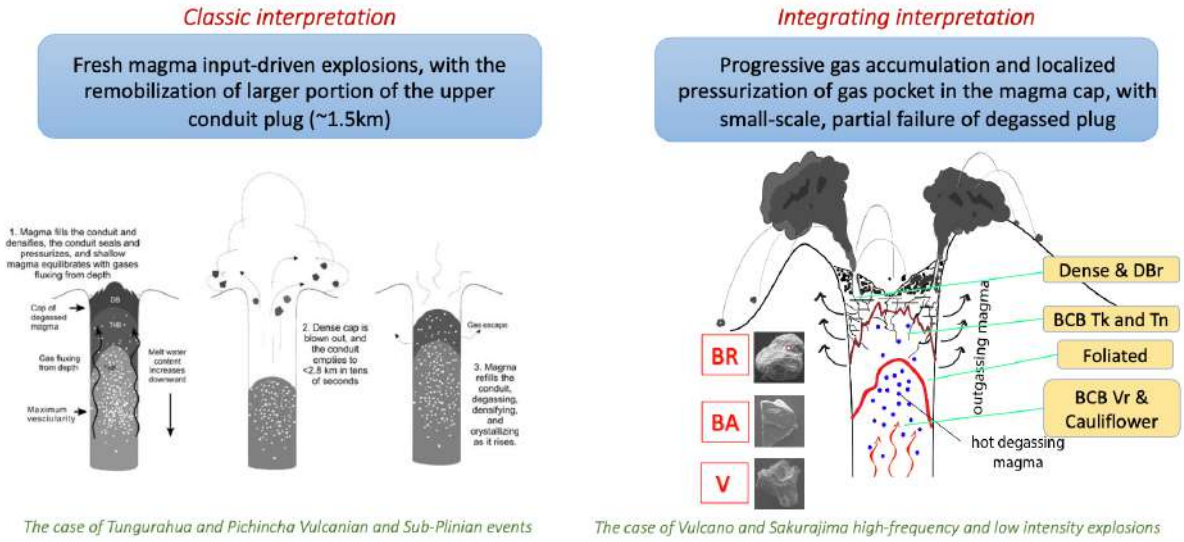

Figure 10: *The proposed, alternative models of vulcanian activity*

6.Third Section - UNINA

6.1 Refining the Late Quaternary tephrostratigraphic framework of the Neapolitan volcanic district from a marine core in the Gulf of Salerno (Tyrrhenian Sea).

6.1.1 Aims

Within the framework of Objective 1 (*A better understanding of environmental, natural and anthropic risks, as well as their interrelation with the effect of climate change*), improving our knowledge of the eruptive history of volcanic sources is essential for robustly assessing volcanic hazards. Key information includes the frequency and magnitude of eruptive events. In regions with recent and active volcanism, such as the Campania Plain, this is further complicated by urbanised areas, which increase the risk to the population and reduce the number of accessible outcrops for data collection.

6.1.2 Results

To expand the existing database, Table 1 was produced to summarise the results provided by the study of 272 samples extracted from marine core C106. Of these, 61 were identified as suitable for geochemical analysis of glass component. These analyses allowed the determination of the eruptive source responsible for the deposition of the individual layers, and the identification of the specific eruptive event in most cases. Several layers were attributed to eruptions that had not previously been recognised. By constructing an age-model based on eight radiocarbon dates and four tie points, which correspond to volcanic eruptions for which precise ages are available in the literature, we were able to assign reliable ages to previously unrecognized events as well as to eruptions with no prior dating. This approach also allowed us to refine the age range of previously known eruptions.

Within core C106, clusters of eruptive events were identified in relation to major eruptions from the Campi Flegrei. The most notable example is the presence of at least three distinct cryptotephra layers in the time span immediately preceding the emplacement of the Neapolitan Yellow Tuff. For these tephra we adopted the definition of "precursors of the Neapolitan Yellow Tuff".

Although belonging to the Tufi Biancastri series, they represent a very brief interval immediately before the caldera-forming eruption. Their role is comparable to that of the four tephra layers from Campi Flegrei, which were deposited over the ~600 years leading up to the Campanian Ignimbrite (Wutke et al., 2015). Due to their highly similar chemical signatures and the limited time span of deposition, these precursors can pose significant challenges when attempting to correlate distal tephra layers but their existence is essential to better resolve the period prior to a caldera-forming eruption. In fact, this supports the hypothesis that such major eruptions may be preceded by clusters of smaller-scale events, rather than by long-term quiescence of the volcanic system refining the hazard assessment for Campi Flegrei.

Regarding Vesuvius, one of the main results for hazard assessment comes from the analysis of the uppermost section of core C106. Between the 472 and 1631 CE eruptions, we recognized three distinct eruptive events (see Table 1). The event dating to around 1572 CE challenges the long-held assumption of an extended period of quiescence prior to the 1631 eruption (Principe et al., 2004). This observation has significant implications, as early hazard assessments and risk mitigation strategies have traditionally been based on the idea that approximately 500 years of volcanic inactivity preceded 1631 (e.g. Bertagnini et al., 2006). Furthermore, these new data suggest that the recurrence rate of moderately explosive eruptions may need to be reassessed as potentially higher than previously estimated. Finally, core C106 provided

evidence of several previously unrecognised eruptive events, which helped to improve our understanding of the timing and recurrence of eruptions on Ischia Island. Among these events, one contemporaneous with the Agnano Monte Spina eruption was identified, and the ages of the Piano Liguori and Cretaio eruptions were refined over the past 10 ka using the age-model. Notably, the Cretaio eruption is now recognized as substantially younger than prior age estimates indicated. These findings allow for a more detailed reconstruction of the volcanic history of Ischia island and provide essential information for probabilistic hazard assessments.

Table 2 - Summary of modelled ages attributed to each cryptotephra using the refined age model, along with their inferred volcanic sources and associated eruptive events. SV= Somma-Vesuvius; CF= Campi Flegrei; IS= Ischia; Pr= Procida; Et= Etna.

Tephra	Source	Event	Modelled age
C106 2-4	SV		
C106 4-6	SV		
C106 6-8	SV	a: GS1/18 b: 1631	
C106 8-10	SV	pre-1631 SV activity	383.1-382.7 (382.9)
C106 24-26	SV	Somma-Vesuvius ca. 1000 CE	932.6-909.3 (919.7)
C106 26-28			
C106 32-34	SV	Somma-Vesuvius ca. 850 CE	1,116-1,085 (1,099)
C106 34-36	SV	Pollena 472 CE	1,178-1,146 (1,160)
C106 46-48	IS	Ischia Cretaio	1,575-1,548 (1,560)
C106 118-120	SV	Pompei 79 CE	
C106 120-122			
C106 122-124			
C106 124-126			
C106 132-134	SV	AP3α or AP4α?	2,735-3,049 (2,894)
C106 138-140			3,000-3,349 (3,180)
C106 144-146	SV	AP3	3,331-3,615 (3,481)
C106 148-150			
C106 166-168	CF	a: Astroni group b: CF unknown	3,733-3,852 (3,792)
C106 168-170			3,838-3,911 (3,871)
C106 172-174			3,955-3,980 (3,962)
C106 176-178	CF	Averno 2	4,066-4,087 (4,070)
C106 188-190	CF+IS	a: AMS b: Ischia unknown	
C106 206-208	IS	Piano Liguori 2	6,207-6,647 (6,438)
C106 214-216	IS	Piano Liguori 1	6,658-7,135 (6,903)
C106 266-268	SV	unknown GM eruption	9,382-9,775 (9,585)
C106 274-276	SV+CF	a: GS1/6a b: Pigna San Nicola	9,730-10,150 (9,950)
C106 304-306	CF	a and b: Agnano Pomici Principali cluster	
C106 308-310	CF	a and b: Agnano Pomici Principali cluster	
C106 318-320	CF	a and b: Agnano Pomici Principali cluster	10,902-11,455 (11,160)
C106 324-326	CF	a and b: Agnano Pomici Principali cluster	
C106 328-330	CF	a and b: Agnano Pomici Principali cluster	
C106 332-334	CF	Agnano Pomici Principali	
C106 334-336	CF	Soccavo 1	12,289-12,543 (12,424)
C106 338-340			
C106 358-360	CF	Neapolitan Yellow Tuff	13,509-14,167 (13,846)
C106 360-362			13,628-14,327 (13,984)
C106 362-364			13,746-14,482 (14,120)
C106 366-368	CF	Precursors of the NYT	13,979-14,770 (14.381)
C106 370-372	CF		
C106 372-374	CF		
C106 374-376	CF		14,433-15,268 (14,858)
C106 376-378	CF		
C106 378-380	CF		
C106 382-384	CF		
C106 384-386	CF		14,967-15,823 (15,404)
C106 386-388	CF		
C106 392-394	CF	Tufi Biancastri Pra	15,375-16,229 (15,811)
C106 412-414	IS+Et	a: Ischia Sant'Angelo cluster b:Etna TM-11 type Y-1	16,357-17,151 (16,760)
C106 414-416	IS+Et+CF	a: Ischia Sant'Angelo cluster b: Etna TM-11 type Y-1c: Tufi Biancastri series	16,455-17,240 (16,853)
C106 416-418	IS	Ischia Sant'Angelo cluster	16,553-17,328 (16,945)
C106 418-420	CF+IS	a: CF unknown b: Ischia Sant'Angelo	16,651-17,417 (17,038)
C106 424-426	CF	Tufi Biancastri series	16,949-17,684 (17,319)
C106 458-460	CF	Tufi Biancastri series	18,830-19,397 (19,106)
C106 464-466	CF	Tufi Biancastri series	19,215-19,765 (19,482)
C106 504-506	CF	Torregaveta	22,508-23,069 (22,775)
C106 512-514	Pr+CF	a: Solchiaro b: C-5	23,290-23,872 (23,566)
C106 520-522	IS	Ischia undefined	24,094-24,700 (24,381)
C106 560-562	CF	Tufi Biancastri series	28,186-28,922 (28,531)
C106 566-568	CF+IS	a: Y3 b: Ischia CET1-crypto 6	28,675-29,424 (29,026)
C106 586-588	CF	Y3	29,532-30,300 (29,892)
C106 616-618	SV	Codola	32,186-33,015 (32,571)

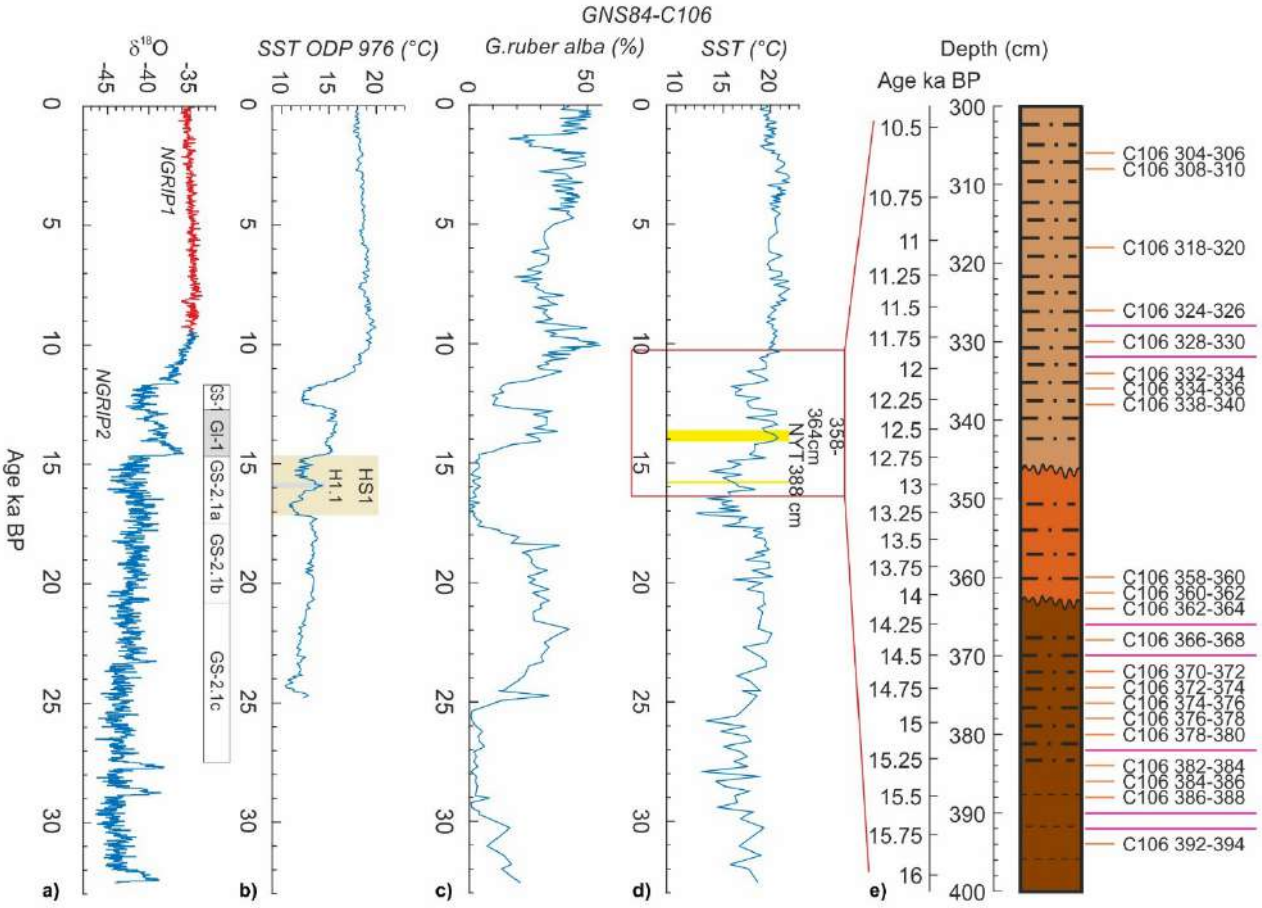

Figure 11: **a)** Isotopic record of the Greenland NGRIP ice core (Rassmussen et al., 2014) and **b)** Sea Surface Temperatures (SSTs) recorded by alkenones at ODP Site 976 in the Alboran Sea (Martrat et al., 2014), in relation to **c)** the percentage abundance of warm water species Globigerinoide ruber (Jamka, 2019) and **d)** SSTs recorded by planktonic foraminiferal assemblages of the C106 core (Di Donato et al., 2019); **e)** Magnification of the 300–400 cm interval of the core, in which the identified cryptotephra (orange lines and sample codes) and the levels where the glass fraction is absent or very low in relation to the non-volcanic component (purple lines) are evident. The beige shading defines Heinrich Stadial HS1 and gray shading layer H1.1 (from Hodell et al., 2017). The yellow shading highlights the deposition of the "precursors of the Neapolitan Yellow Tuff" and of the NYT itself.

6.2 Unravelling 6000 years of interplay among environmental changes, anthropogenic activities, and Vesuvius eruptions in the upper Sarno Plain (Campania, Italy).

6.2.1 Aims

Within the framework of Objective 1 (*A better understanding of environmental, natural and anthropic risks, as well as their interrelation with the effect of climate change*), we carried out a multiproxy investigation on a lacustrine sequence of the inner Sarno plain (B24 drill hole) in the San Vito area. The main aims of the investigation were: i) scanning the sequence of landscape and land use changes by combining paleoenvironmental, tephrostratigraphical, chronological and archaeological/historical data and ii) highlighting the direct and/or indirect impact of volcanic eruptions on the environment and human activities in the upper Sarno Plain.

6.2.2 Results

The plain of the Sarno River (Campania, Italy) is especially known for the presence of *Pompeii*, the world's most famous archaeological site of the Roman age. This town was completely buried by the Plinian eruption of the Somma-Vesuvius volcano in CE 79, which also destroyed the towns of *Herculaneum*, *Stabiae* and the houses and farms distributed throughout the territory directly affected by the volcanic products. For this reason, starting from the first excavations of Pompeii and Herculaneum at the end of 18th century, scholars have mainly focused their studies on the buried cities and remains as well as on the coastal plain area, where most of these are found. The scarcity of data on the past environment and landscape of the Sarno Plain is related to the difficulty of finding successions suitable in an alluvial environment rich in repeated primary and secondary volcanic inputs. The discovery in the inner sector of the plain of a thick lacustrine deposit, whose base is older than 5500 years (Santo et al., 2019), has provided an exceptional opportunity to study in detail the environmental evolution of this area over the past millennia. The presence of numerous Campi Flegrei and Somma-Vesuvius primary and reworked volcanic levels also provided the dual opportunity to refine the chronology of the fill and to study the effects of eruptions on vegetation and human activities. Reworked tephra can make chronostratigraphic reconstructions very difficult, but when the age and extent of reworking are accurately retraceable, as in the sequence here presented, the reworked materials derived from tephra may provide a viable secondary isochron (Lowe, 2011). This study provides the first well-dated long history of environmental and land use changes in the Sarno Plain.

The recovery at the footslope of the Sarno Mts. of a lacustrine succession covering the last 6000 years, gave us the exceptional opportunity to provide a valuable pollen record for the Campania region. The integrated use of ^{14}C ages and tephrostratigraphy for the construction of a robust chronology had the advantage of crosschecking between the two datasets. We demonstrated that most of the reworked volcaniclastic layers were emplaced soon after the eruptive events and thus their “first appearance” in the sedimentary record could be used as a chronological marker (Fig. 3). This approach allowed us to assign an age of ca. 3100 cal yr BP to the protohistoric eruption AP4, hitherto poorly dated as younger than 2800 cal yr BP.

The chronology allowed scanning human activities in the different cultural periods, demonstrating the long-standing resilience of the populations that have inhabited this territory, which also interacted with the occurrence of numerous volcanic, even catastrophic, events. In-depth archaeological and historical knowledge has been essential to attributing variations in land use to a particular cultural facies and thus determining their major activities in the spatial setting.

Despite the upper Sarno Plain was only reached by reduced thickness of pyroclastic fall deposits, it was indirectly influenced by the major eruptions that affected the southwestern sector of the plain, where the main economic centres developed both in Protohistoric and Roman times. In fact, our results show that, as expected, a thickness of pyroclastic fall tephra in the order of 10 cm did not affect either the tree cover or human activities in any significant way. On the other hand, the total destruction of the built environment and of social links, due to the large number of victims in the main towns during the CE 79 eruption, had a

strong impact also outside the area directly affected by the lethal pyroclastic currents. This result can provide useful information for defining the limits of the area exposed to the indirect effects of a possible future eruption.

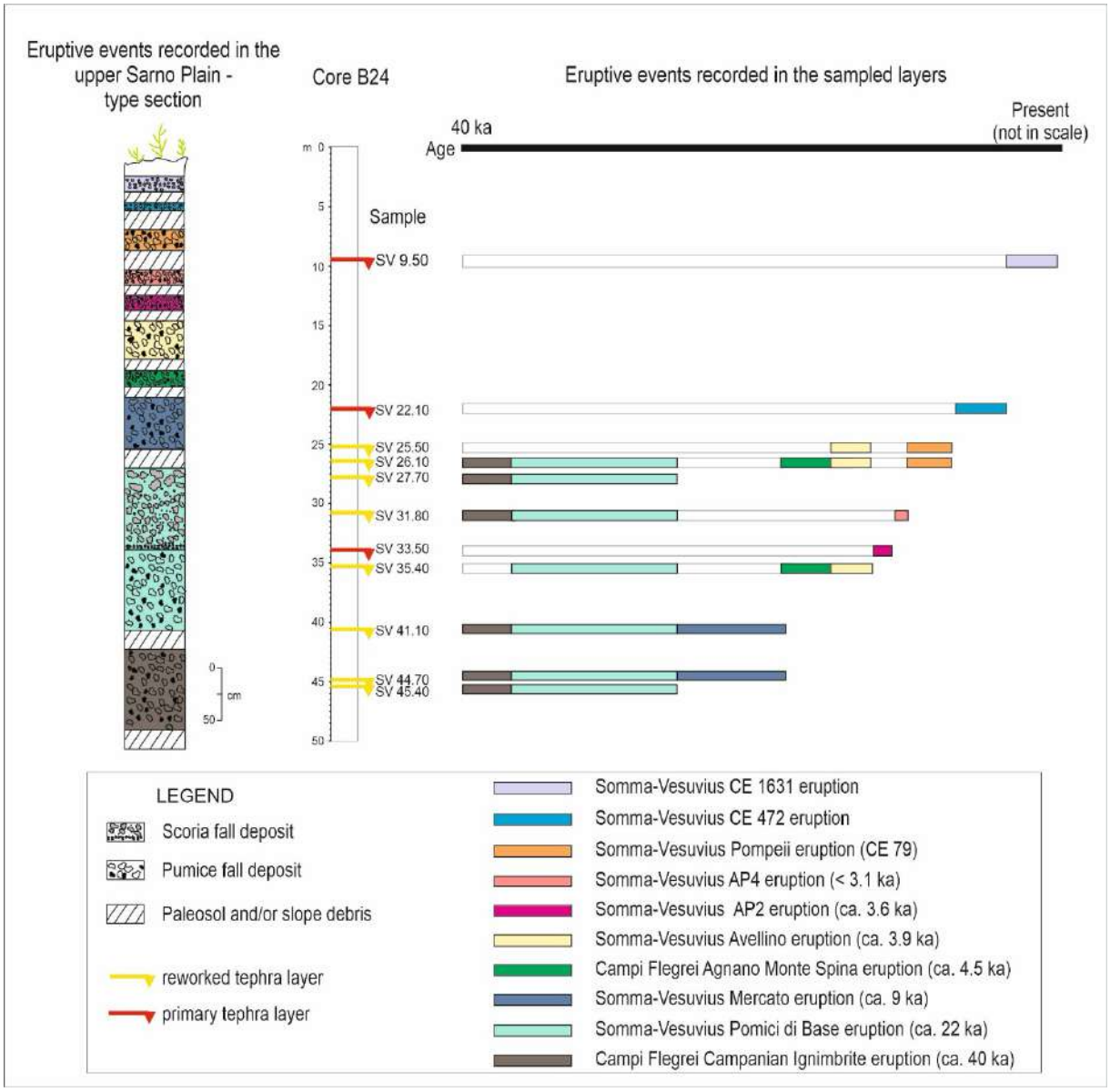

Figure 12: Left: type section of the pyroclastic fall deposits cropping out in upper Sarno Plain. The thickness of the single layers is the maximum recorded in the area. Right: plot of the eruptions found in the San Vito succession; red flag=primary tephra (mono-component); yellow flag= reworked tephra (poly-component).

Table 2: Summary of the attribution of the primary and reworked tephra embedded in the San Vito sequence, with the age constraints derived from tephrostratigraphic analysis. Abbreviations: Tr=trachyte; Tr-ph= trachy-phonolite; Ph=phonolite; Tph=tephriphonolite; Ph-teph=phonotephrite; Foi=foidite. [1]Santacroce et al. (2008); [2]Giaccio et al. (2017); [3]Passariello et al. (2009); [4]Smith et al. (2011); [5]Totaro et al. (2022) and references therein.

Sample	Reworked/ Primary tephra	Cluster	Type of juvenile fragments	Chemical composition	SiO_2 wt%	K_2O/Na_2O	eruption	Age	Age of the layer
SV 45.4	Reworked	2	pumice	Tr-ph	61.7-57.6	>2.0	Pomici di Base	ca. 22 ka[1]	Not younger than 22 ka
		1	pumice	Tr-ph	ca. 61	ca. 1.1	Campanian Ignimbrite	ca. 40 ka[2]	
SV 45.4	Reworked	3	pumice	Ph	59	ca. 0.9	Mercato	ca. 9 ka[1]	Not younger than 22 ka
		2	pumice	Tr-ph	61.7-57.6	>2.0	Pomici di Base	ca. 22 ka[1]	
		1	pumice	Tr-ph	ca. 61%	ca. 1.1	Campanian Ignimbrite	ca. 40 ka[2]	
SV 41.6	Reworked	3	pumice	Ph	59	ca. 0.9	Mercato	ca. 9 ka[1]	Not younger than 9 ka
		2	pumice	Tr-ph	61.7-57.6	>2.0	Pomici di Base	ca. 22 ka[1]	
		1	pumice	Tr-ph	ca. 61%	ca. 1.1	Campanian Ignimbrite	ca. 40 ka[2]	
SV 35.4	Reworked	3	pumice	Ph	57.6-54.6	0.74-1.35	Avellino	3870 cal yrs BP[3]	Not younger than 3.87 ka
		2	pumice	Tr	ca. 60	ca. 2.3	Agnano Monte Spina	ca. 4.5 ka[4]	
		1	pumice	Tr-ph	61.7-57.6	>2.0	Pomici di Base	ca. 22 ka[1]	
SV 33.5	Primary		pumice	Ph	ca. 56	1.00-1.79	AP2	3615 cal yrs BP	3.38 ka
SV 31.8	Reworked	3	leucite bearing pumice	Ph-tph	ca. 54	0.8-1.6	AP4	Uncertain age	Not younger than ca. 3.3 ka[5]
		2	pumice	Tr-ph	61.7-57.6	>2.0	Pomici di Base	ca. 22 ka[1]	
		1	pumice	Tr-ph	ca. 61%	ca. 1.1	Campanian Ignimbrite	ca. 40 ka[2]	
SV 27.7	Reworked	2	pumice	Tr-ph	61.7-57.6	>2.0	Pomici di Base	ca. 22 ka[1]	Not useful to provide age constraints
		1	pumice	Tr-ph	ca. 61	ca. 1.1	Campanian Ignimbrite	ca. 40 ka[2]	
SV 26.1	Reworked	4	leucite bearing pumice	Ph	ca. 55	0.98-1.49	79 CE	79 CE	Not younger than 79 CE
		3	aphyric pumice	Ph	57.6-54.6	0.69-0.77	Avellino	3870 cal yrs BP[3]	
		2	pumice	Tr	ca. 60	ca. 2.3	Agnano Monte Spina	ca. 4.5 ka[4]	
		1	pumice	Tr-ph	ca. 61	ca. 1.1	Campanian Ignimbrite	ca. 40 ka[2]	
SV 25.5	Reworked	2	leucite bearing pumice	Ph	ca. 55	0.98-1.49	79 CE	79 CE	Not younger than 79 CE
		1	aphyric pumice	Ph	57.6-54.6	0.69-0.77	Avellino	3870 cal yrs BP[3]	
SV 22.5	Primary		scoria	Foi to Ph-teph	48.1-52.6	ca. 0.8	Pollena	472 CE	472 CE
SV 9.50	Primary		scoria	Low-silica ph	ca. 54	0.79-1.13	1631 CE	1631 CE	1631 CE

7. Conclusions

This deliverable presents an integrated reconstruction of the impact and initial conditions of explosive eruptions through the reverse engineering of pyroclastic deposits, within the framework of WP3.3 . By combining field-based volcanology, stratigraphic and structural analysis, laboratory investigations, geochemical characterization, geochronology, and innovative three-dimensional imaging techniques, the project provides new constraints on eruption triggering mechanisms, conduit processes, and eruptive impacts across different volcanic settings.

The investigations conducted at Milos and Nisyros islands significantly advance the understanding of phreatic and hydrothermal explosive activity. At Milos, the identification and characterization of numerous small craters demonstrate that repeated shallow steam-driven explosions can occur in low-enthalpy hydrothermal systems under conditions of localized overpressure and structural control. The recognition of exceptionally large phreatic events, such as those responsible for the so-called Green Lahar deposit, expands the known magnitude spectrum of steam-driven eruptions and highlights their potential for widespread proximal impacts. At Nisyros, detailed stratigraphic reconstruction integrated with UAV-based mapping and structural analysis reveals the composite nature of major craters and the strong tectonic influence on vent localization. Together, these studies refine conceptual models of hydrothermal sealing, pressurization, and explosive failure in caldera-hosted systems.

Research at Vulcano Island provides a detailed reconstruction of late Holocene eruptive activity at La Fossa cone, with particular emphasis on the mechanisms governing vent opening and early eruptive transitions. Stratigraphic, textural, and geochemical analyses demonstrate recurrent shifts from phreatic to hydromagmatic and magmatic activity, controlled by magma plug dynamics and volatile exsolution. The study of the 1888–1890 ballistic bomb field reveals that dense, microlite-rich blocks constitute the dominant ejecta type, indicating the formation of a degassed upper magma plug as a key condition for vulcanian explosions. Textural evidence from breccia-bearing blocks further suggests that non-explosive shear-related fragmentation and fracture-controlled degassing played a major role during low-intensity phases. Comparative analysis with other vulcanian eruptions confirms the existence of a spectrum of behaviors governed by plug evolution and pressurization dynamics, providing a robust reference framework for future hazard assessment scenarios.

The UNIFI contribution introduces a novel methodological approach for the three-dimensional characterization of volcanic ash aggregates. The development of a system capable of preserving fragile airborne aggregates and reconstructing their internal structure through X-ray tomography provides, for the first time, quantitative data on morphology, porosity, and density of natural aggregates. These parameters are essential for improving atmospheric transport and ash dispersal models, with direct implications for aviation safety, public health, and distal hazard forecasting.

Finally, the high-resolution tephrostratigraphic investigations in the Neapolitan volcanic district refine eruption chronologies and improve constraints on recurrence rates and eruptive clustering. The analysis of marine and lacustrine sequences identifies previously unrecognized eruptive events and provides evidence that major caldera-forming eruptions may be preceded by clusters of smaller-scale activity rather than prolonged quiescence. Moreover, the integration of paleoenvironmental and archaeological data demonstrates that moderate tephra fallout had limited ecological impact, whereas the indirect socio-economic consequences of major eruptions extended beyond areas directly affected by destructive pyroclastic currents.

Overall, the reverse engineering of pyroclastic deposits confirms its fundamental role in reconstructing eruptive dynamics, subsurface conditions, and impact scenarios. The results achieved in Deliverable DV 3.3.2 provide improved constraints on explosion energy, excavation depth, ballistic dispersal, aggregation processes, and eruption recurrence. These advances strengthen the scientific basis for probabilistic hazard assessment and contribute to the broader objective of enhancing resilience in volcanic regions within the RETURN project framework.

8. References

Bertagnini, A., Cioni, R., Guidoboni, E., Rosi, M., Neri, A., Boschi, E. (2006) Eruption early warning at Vesuvius: the A.D. 1631 lesson. Geophysical Research Letters, 33, L18317. https://doi.org/10.1029/2006GL027297

Di Donato, V., Jamka, J., Martín-Fernández, J.A. (2019) Compositional Regression-Based methods for SST reconstruction. Alpine and Mediterranean Quaternary, 32 (1), 31-41. https://doi.org/10.26382/AMQ.2020.02

Giaccio, B., Hajdas, I., Isaia, R., Deino, A., Nomade, S. (2017). High-precision ^{14}C dating and $^{40}Ar/^{39}Ar$ dating of the Campanian Ignimbrite (Y-5) reconciles the time-scales of climatic-cultural processes at 40 ka. Scientific Reports, 7, 45940. https://doi.org/10.1038/srep45940

Hodell, D.A., Nicholl, J.A., Bontognali, T.R.R., Danino, S., Dorador, J., Dowdeswell, J.A., Einsle, J., Kuhlmann, H., Martrat, B., Mleneck-Vautravers, M.J., Rodríguez-Tovar, F.J., Röhl, U. (2017) Anatomy of Heinrich Layer 1 and its role in the last deglaciation. Paleoceanography, 32, 284–303 https://doi.org/10.1002/2016PA003028

Jamka, J.M., (2019) High resolution integrated reconstruction of Holocene climatic and paleoenvironmental changes in the southern Tyrrhenian sea: a coda approach. PhD Thesis University of Napoli Federico II, 218 pp.

Lowe, D.J. (2011) Tephrochronology and its application: a review. Quaternary Geochronology, 6, 107–153. https://doi.org/10.1016/j.quageo.2010.08.003

Martrat, B., Jimenez-Amat, P., Zahn, R., Grimalt, J.O., (2014) Similarities and dissimilarities between the last two deglaciations and interglaciations in the North Atlantic region. Quaternary Science Reviews, 99, 122–134. https://doi.org/10.1016/j.quascirev.2014.06.016

Passariello, I., Albore Livadie, C., Talamo, P., D'Onofrio, A., Terrasi, F. (2009) ^{14}C Chronology of the Avellino Pumices eruption and timing of human reoccupation of the devastated region. Radiocarbon 51(2): 803–816. https://hal.science/hal-03929497v1

Principe, C., Tanguy, J-C., Arrighi, S., Paiotti, A., Le Goff, M., Zoppi, U. (2004) Chronology of Vesuvius' activity from A.D. 79 to 1631 based on archeomagnetism of lavas and historical sources. Bulletin of Volcanology, 66, 703-724. https://doi.org/10.1007/s00445-004-0348-8

Rasmussen, S.O., Bigler, M., Blockley, S.P., Blunier, T., Buchardt, S.L., Clausen, H.B., Cvijanovic, I., Dahl-Jensen, D., Johnsen, S.J., Fischer, H., Gkinis, V., Guillevic, M., Hoek, WZ., Lowe, J.J., Pedro, J.B., Popp, T., Seierstad, I.K., Steffensen, J.P., Svensson, A.M., Vallelonga, P., Vinther, B.M., Walker, M.J.C., Wheatley, J.J., Winstrup, M. (2014) A stratigraphic framework for abrupt climatic changes during the Last Glacial period based on three synchronized Greenland ice-core records: refining and extending the INTIMATE event stratigraphy. Quaternary Science Reviews, 106, 14-28. https://doi.org/10.1016/j.quascirev.2014.09.007

Santacroce, R., Cioni, R., Marianelli, P., Sbrana, A., Sulpizio, R., Zanchetta, G., Donahue, D.J., Joron, J.L. (2008) Age and whole rock–glass compositions of proximal pyroclastics from the major explosive eruptions of Somma-Vesuvius: a review as a tool for distal tephrostratigraphy. Journal of Volcanology and Geothermal Research, 177, 1-18. https://doi.org/10.1016/j.jvolgeores.2008.06.009

Santo, A., Santangelo, N., De Falco, M., Forte, G., Valente, E. (2019) Cover collapse sinkhole over a deep buried carbonated bedrock: The case study of Fossa San Vito (Sarno – Souther Italy). Geomorphology, 345, 106838. https://doi.org/10.1016/j.geomorph.2019.106838

Smith, V.C., Isaia, R., Pearce, N.J.G. (2011) Tephrostratigraphy and glass compositions of post-15 kyr Campi Flegrei eruptions: implications for eruption history and chronostratigraphic markers. Quaternary Science Reviews, 30, 3638-3660. https://doi.org/10.1016/j.quascirev.2011.07.012

Totaro, F., Insinga, D.D., Lirer, F., Margaritelli, G., Català i Caparrós, A., de la Fuente, M., Petrosino, P. (2022) The Late Pleistocene to Holocene tephra record of ND14Q site (southern Adriatic Sea):

Traceability and preservation of Neapolitan explosive products in the marine realm. Journal of Volcanology and Geothermal Research, 423, 107461. https://doi.org/10.1016/j.jvolgeores.2021.107461

Wutke, K., Wulf, S., Tomlinson, E.L., Hardiman, M., Dulski, P., Luterbacher, J., Brauer, A. (2015) Geochemical properties and environmental impacts of seven Campanian tephra layers deposited between 40 and 38 ka BP in the varved lake sediments of Lago Grande di Monticchio, southern Italy. Quaternary Science Reviews, 118, 67-83. https://doi.org/10.1016/j.quascirev.2014.05.017

USE APA style https://apastyle.apa.org/style-grammar-guidelines/references/examples

SEE Examples below

TEXTUAL WORK

Grady, J. S., Her, M., Moreno, G., Perez, C., & Yelinek, J. (2019). Emotions in storybooks: A comparison of storybooks that represent ethnic and racial groups in the United States. Psychology of Popular Media Culture, 8(3), 207–217. https://doi.org/10.1037/ppm0000185

Kushilevitz, E., & Malkin, T. (Eds.). (2016). Lecture notes in computer science: Vol. 9562. Theory of cryptography. Springer. https://doi.org/10.1007/978-3-662-49096-9